Ab initio calculation of the vibrational modes of SiH_4, H_2SiO, $Si_{10}H_{16}$, and $Si_{10}H_{14}O$

2008 J. Phys.: Condens. Matter 20 224013

(http://iopscience.iop.org/0953-8984/20/22/224013)

J. Phys.: Condens. Matter **20** (2008) 224013 (6pp) doi:10.1088/0953-8984/20/22/224013

Ab initio calculation of the vibrational modes of SiH_4, H_2SiO, $Si_{10}H_{16}$, and $Si_{10}H_{14}O$

Katalin Gaál-Nagy, Giulia Canevari and Giovanni Onida

European Theoretical Spectroscopy Facility (ETSF), CNR-INFM and Dipartimento di Fisica, Università degli Studi di Milano, via Celoria 16, I-20133 Milano, Italy

E-mail: katalin.gaal-nagy@physik.uni-regensburg.de

Received 8 November 2007, in final form 7 February 2008
Published 13 May 2008
Online at stacks.iop.org/JPhysCM/20/224013

Abstract

We have studied the normal modes of hydrogenated and oxidized silicon nanocrystals, namely SiH_4 (silane), H_2SiO (silanone), $Si_{10}H_{16}$, and $Si_{10}H_{14}O$. The small clusters (SiH_4 and H_2SiO) have been used for convergence tests and their bond-lengths and frequencies have been compared with experimental and theoretical reference data. For the large clusters ($Si_{10}H_{16}$ and $Si_{10}H_{14}O$) we have investigated the vibrational density of states, where we have identified the oxygen-related spectral features. The vibrational modes have also been analyzed with respect to the displacement patterns. The calculations have been carried out within the density-functional and density-functional perturbation theory using the local-density approximation.

(Some figures in this article are in colour only in the electronic version)

1. Introduction

Silicon nanostructures have important applications in microelectronics due to the downscaling of optoelectronic devices. Because of this, the optical, electronic, and vibrational properties of these systems are of great interest. For example, photoluminescence of quantum wires has been discovered [1]. The investigation of silicon nanocrystals is another step in the direction of the development of nanostructured devices. Although the electronic and optical properties of oxidized and non-oxidized nanocrystals have been studied extensively [2–6], much less is known about their vibrational properties. Nevertheless, the production and operation of devices is carried out at room temperature, where the vibrations of the crystals play an important role. They can enhance adsorption processes as well as influencing the optical properties of the systems.

$Si_{10}H_{16}$ and $Si_{10}H_{14}O$ are good models for the study of (oxidized) miniaturized semiconductors, since they are simple and they can be studied with fully *ab initio* total energy calculations. Thus, we have studied the vibrational properties for these systems as prototypes for non-oxidized and oxidized nanocrystals. Besides the influence of the dynamics of the nanocrystals on chemical processes, their vibrational frequencies can also be utilized for the characterization of the oxidized clusters due to the signature of the oxygen in the vibrational density of states. In a first step we have studied smaller systems (silane and silanone) to assess the numerical convergence. Furthermore, for silane and silanone experimental and theoretical reference data exist, which can be used for comparison.

This article is organized as follows. After a short description of the method employed in our calculations, we present the results for silane and silanone (section 3), where the convergence tests, an analysis of the displacement patterns, and a comparison with experimental and theoretical results are shown. Then, we investigate $Si_{10}H_{16}$ and $Si_{10}H_{14}O$ (section 4). Here, we discuss again some convergence issues before going to the final results for the vibrational density of states, which have been analyzed with respect to oxygen-related features and their displacement patterns. Finally, we summarize and draw a conclusion.

2. Method

All calculations have been carried out with the ABINIT package [7]. It is based on a plane-wave pseudopotential approach to the density-functional theory (DFT) [8, 9]. We have employed norm-conserving pseudopotentials in

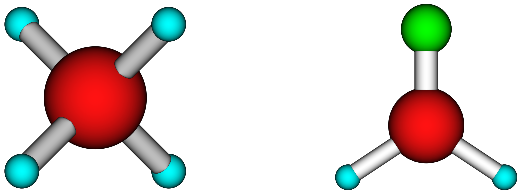

Figure 1. Silane (left) and silanone (right). Silicon atoms are drawn with large (dark-red) spheres, hydrogen atoms with small (light-blue) ones, and oxygen atoms with medium-sized (green) ones.

the Troullier–Martins style [10]. The exchange–correlation energy is described within the local-density approximation (LDA) [11, 12]. The phonon frequencies have been calculated utilizing the density-functional perturbation (DFPT) scheme [13, 14]. Since we apply a plane-wave method to an isolated system we have used the supercell method and the Γ point only in the **k** point sampling. The atomic positions have been relaxed till the residual forces are less than 0.5 mHa/a_B.

3. Silane and silanone

In a first step we have studied silane (SiH_4) and silanone (H_2SiO) as the smallest oxidized and non-oxidized silicon clusters. The atomic structure is shown in figure 1. Both systems are highly symmetric, with space groups T_d and C_{2v}, respectively. This yields in part a degeneracy of the vibrational frequencies.

The small molecules have been utilized for the convergence tests (section 3.1), since the investigation of big crystals is more time consuming. However, the displacement patterns for the various vibrational modes have also been analyzed (section 3.2), and the resulting frequencies have been compared with reference values (section 3.3).

3.1. Convergence tests

Applying a plane-wave approach together with a supercell method, the two main convergence parameters in the calculation are the kinetic energy cutoff (E_{cut}), which determines the number of plane waves used in the expansion, and the size of the (cubic) supercell, meaning the amount of vacuum around the isolated cluster. The latter parameter should be chosen as small as possible in order to reduce the computational effort, but large enough in order to avoid an interaction of the neighboring clusters, since periodic boundary conditions are employed.

The results for the variation of the total energy E_{tot} as a function of the supercell lattice parameter (a_{cell}) and as a function of E_{cut} are shown in figure 2. We have performed the convergence tests with respect to E_{cut} for both silane and silanone, since the description of the oxygen requires a larger number of plane waves than for the other atoms. As visible in the figure, the size of the supercell has a rather small influence on the calculation. The variation of E_{tot} is in the μHa range and therefore we have chosen $a_{cell} = 30\ a_B$. The variation of E_{tot} with respect to the number of plane waves is larger. For silane, convergence has been achieved at $E_{cut} = 17.5$ Ha, yielding an error of less than 0.4 mHa in E_{tot}. Compared with silane the total energy of silanone converges a factor of 10 slower. At $E_{cut} = 32.5$ Ha we found a difference of less than 1.5 mHa compared with the value of E_{tot} at absolute convergence. Thus, $E_{cut} = 32.5$ Ha is sufficient for the numerical description of silanone.

Since we want to investigate the vibrational excitations, we also inspected the frequencies of silane and silanone. The lowest six frequencies, the translational and rotational ones, should vanish. Due to the numerical noise and incompleteness of the plane-wave basis set, these frequencies do not vanish exactly. However, in the case of silanone, which is less converged with respect to the number of plane waves, they have values less than 18 cm^{-1}, which is sufficiently small. For silane they are even smaller.

3.2. Eigenvectors for silane and silanone

The vibrations of silane and silanone can be characterized by their displacement patterns. Silane has 15 vibrational modes, where six are vanishing. Analyzing the frequencies, we found that the lowest frequency is threefold, the next twofold, and the highest threefold degenerate due to the symmetry of the system. The eigendisplacements are shown in figure 3. There are two scissor and two stretching patterns, where in each case there is a symmetric displacement and an asymmetric one.

For silanone we have in total 12 frequency eigenvalues; of these six are vanishing. The remaining six true vibrations show no degeneracy. As for silane, we have inspected the eigenvectors of silanone, which are displayed in figure 4. Besides the two scissor and the two stretching modes, there are two bending modes, where for one the displacement of the hydrogen atoms is in the x–y plane, and for the other it is in the z direction. (Note that the x–y plane is defined as the plane of the planar molecule.) Also here, we have found symmetric and asymmetric modes for the scissor and the stretching mode.

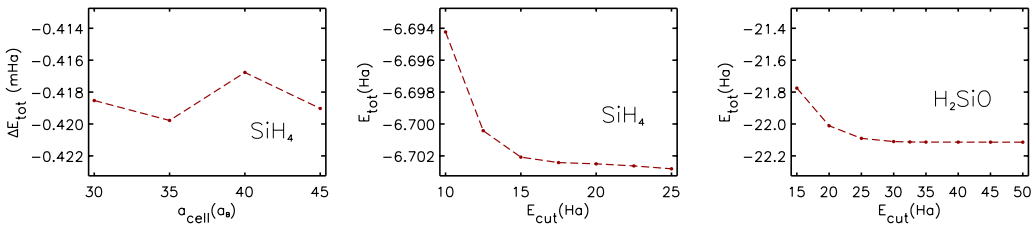

Figure 2. Total energy E_{tot} as a function of the supercell lattice parameter a_{cell} for silane (left), where the total energy is reduced by an offset of 6702 mHa, as a function of the kinetic energy cutoff E_{cut} for silane (middle) and silanone (right). Note that the scale of the total energy in the left figure is in mHa, whereas the scale in the other two figures is in Ha.

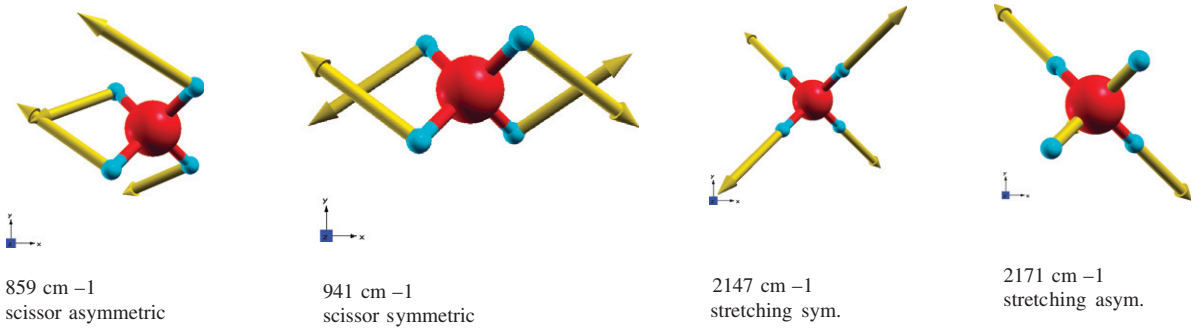

Figure 3. Eigenvectors of silane with symmetric (sym) and asymmetric (asym) displacements for the frequencies denoted in the subsets. For the assignment of the atoms see figure 1.

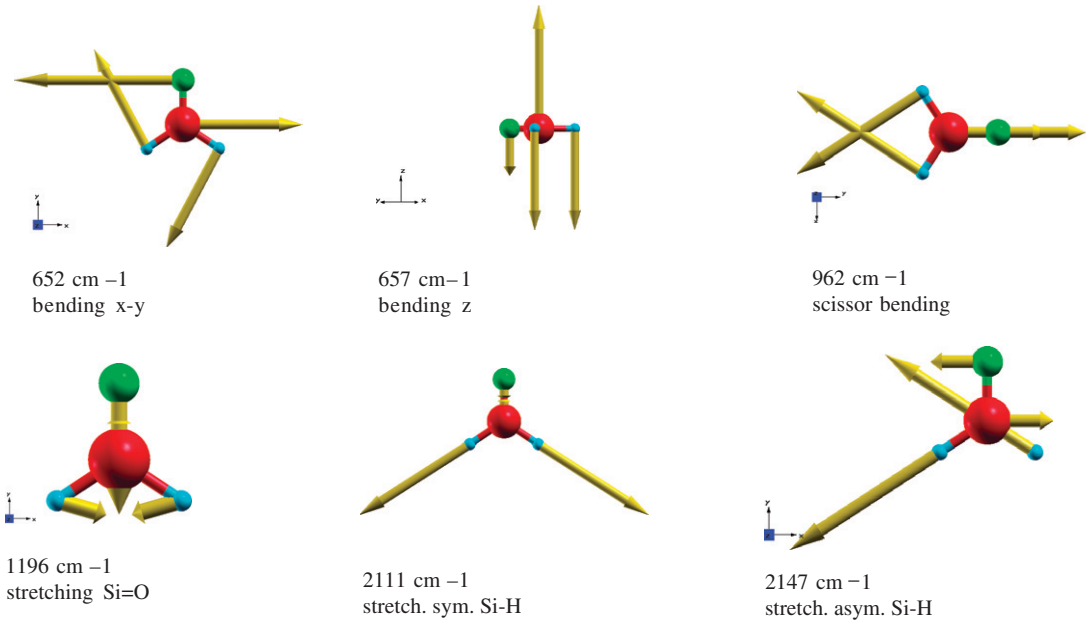

Figure 4. Eigenvectors of silanone with symmetric (sym) and asymmetric (asym) displacements for the frequencies denoted in the figures. The lengths of the oxygen-and silicon-related eigenvectors have been expanded for visibility. For the assignment of the atoms see figure 1.

The stretching modes can be divided in two classes: modes with a large movement of the oxygen and modes where the oxygen is displaced only a little. Usually the displacements of the hydrogens are at least a factor of 10 larger than the ones of the other atoms. Therefore, we have rescaled the eigenvectors of oxygen and silicon in the figure for visibility. There is just one mode where the displacement of the oxygen is of the same order of magnitude as the hydrogens: the stretching Si=O mode. This vibration mode is characteristic for the presence of oxygen in silanone.

Table 1. Calculated bond distance and vibrational frequencies for silane in comparison with experimental results and theoretical (th.) tight-binding data.

Silane	This work	th. [17]	th. [18]	Experiment
Distance Si–H (Å)	1.4872	1.48	1.48	1.4798 [16]
Frequencies (degeneracy) (cm^{-1})				
Scissor asym. (3)	859	871	831	911 [15]
Scissor sym. H–Si–H (2)	941	976	984	976 [15]
Stretching sym. H–Si (1)	2147	2226	2226	2178 [15]
Stretching asym. H–Si (3)	2171	2291		2191 [15]

3.3. Comparison with experimental results

For the small clusters silane and silanone, there are experimental and theoretical reference data available to which we can compare our results. With this comparison we can also prove the reliability of the computational approach used here.

A comparison of our results for silane with the measured data and available theoretical data is presented in table 1. The overall agreement is good; however, the experimental frequencies are slightly underestimated by the calculated ones. The relative difference between the results for the frequencies of Cardona [15] and ours is 6% for the asymmetric scissor mode, 4% for the symmetric one, and 1% for the symmetric and the asymmetric stretching mode. Besides, the agreement of the silicon–hydrogen bond length is excellent. For the lower frequencies the tight-binding results are closer

Table 2. Calculated bond distances and vibrational frequencies for silanone in comparison with experimental (exp.) results and theoretical (th.) ones.

Silanone	This work	th. [21]	th. [22]	th. [23]	exp.
		Distances (Å)			
Si–H	1.491	1.482	1.505	1.478	1.472 [19]
Si=O	1.505	1.517	1.534	1.522	1.515 [19]
		Frequencies (cm^{-1})			
Bending x–y plane	652	706	676	680	697 [20]
Bending z direction	657	712	693	692	
Scissor bending H–Si–H	962	1023	977	993	
Stretching Si=O	1196	1217	1197	1203	1202 [20]
Stretching sym. H–Si	2111	2223	2127	2162	
Stretching asym. H–Si	2140	2238	2132	2186	

to the experimental frequencies; however, these calculations used experimental values for the fitting of the tight-binding parameters whereas our calculation is fully *ab initio*.

For silanone there are just two experimental values available, which have been obtained by infrared spectroscopy of silanone in an Ar matrix [20]: the silicon–oxygen stretching frequency at 1202 cm^{-1} and a frequency at 697 cm^{-1}, where the assignment is not clear. It corresponds either to the bending frequency in the x–y plane or to the one in the z direction. There exist theoretical investigations of the vibrational properties of silanone, based on *ab initio* approaches like molecular-orbital theory, Hartree–Fock, configuration interaction, coupled–cluster methods, and others [21–27]. In these calculations the results vary depending on the method, even sometimes within the same theoretical approach, e.g. just changing the basis set used in the local-orbital expansion. For example, the Si=O stretching frequency has been obtained at 1355 cm^{-1} by Darling and Schlegel [24], 1182 cm^{-1} by Gole and Dixon [22], and 1217 cm^{-1} by Hargittai and Réffy [21], all by using the same expansion into Gaussian functions implemented in GAUSSIAN [28]. Thus, we have compared our results with some of the most recent theoretical values, which are the Gaussian-expansion results using a B3LYP/6-311G(d,p) DFT basis set of Hargittai and Réffy [21], the molecular-orbital theory results using a triple ζ valence basis set at the local DFT level of Gole and Dixon [22], and the coupled cluster method results using a quadruple ζ basis set of Martin [23]. As visible in table 2, the agreement with the theoretical references is very good. Therefore, the vibrational properties of isolated systems can be described very well using a periodic-cell approach based on plane waves instead on local orbitals. Inspecting the results in more detail, our results are very close to the ones of Gole and Dixon [22] also using a density-functional theory approach. Our results are in part closer to the experimental values than the frequencies calculated by other groups.

Last, we can compare the vibrations of silane with those of silanone. Here we found that the Si–H–Si scissor bending and the symmetric and the asymmetric Si–H modes in both systems have very similar frequencies, which differ by less than 2% between silane and silanone. Thus, the intermediate Si=O stretching frequency can be utilized to characterize silanone experimentally.

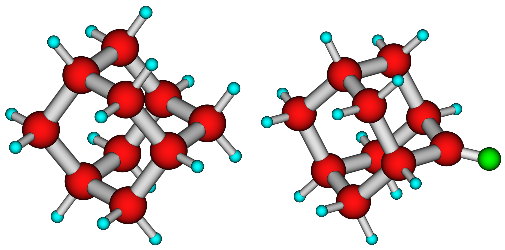

Figure 5. $Si_{10}H_{16}$ (left) and $Si_{10}H_{14}O$ (right). The assignment of the atoms is as in figure 1.

4. $Si_{10}H_{16}$ and $Si_{10}H_{14}O$

The big nanocrystals $Si_{10}H_{16}$ and $Si_{10}H_{14}O$ have been investigated in a similar way to the small ones. $Si_{10}H_{16}$ has the same space group symmetry as silane. It is displayed in figure 5. In $Si_{10}H_{16}$ there are two kinds of silicon atoms: those which are bonded to three other silicon atoms and which have therefore only one dangling bond, which is saturated with a hydrogen atom, and those which are bonded to two other silicon atoms, where two hydrogen atoms are necessary to saturate the bonds. There are various possibilities to oxidize this crystal. The oxygen can be bonded between first- or second-neighbor silicon atoms, where each of the oxygen-bonding silicons will lose one hydrogen. However, we have chosen another configuration for $Si_{10}H_{14}O$ (see figure 5), where the oxygen is double bonded to a silicon atom, yielding the same space group symmetry as silanone. Even if this configuration is not the energetically most favorable one, it is just ≈60 mHa less stable than the most stable one. Since H_2SiO and $Si_{10}H_{14}O$ both have a double-bonded oxygen, one can compare the corresponding Si=O stretching frequencies.

Before investigating the vibrational properties of $Si_{10}H_{16}$ and $Si_{10}H_{14}O$ we want to reinspect the convergence parameters (section 4.1). Afterwards, we analyze the vibrational density of states (section 4.2) and the displacement patterns for oxygen-related modes (section 4.3).

4.1. Convergence

Since $Si_{10}H_{16}$ and $Si_{10}H_{14}O$ are larger than SiH_4 and H_2SiO, it is necessary to increase the size of the supercell from

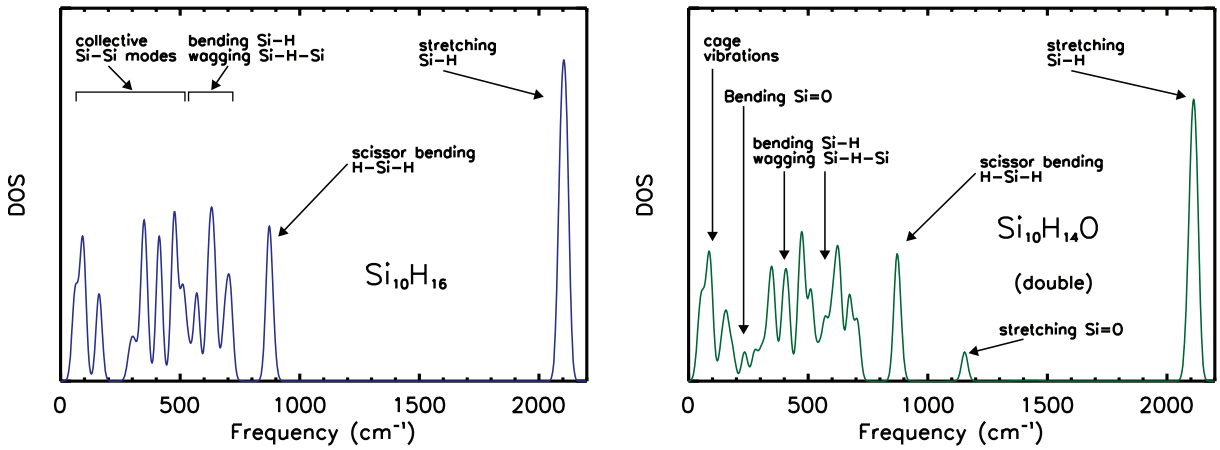

Figure 6. Vibrational density of states (DOS) of $Si_{10}H_{16}$ (left) and $Si_{10}H_{14}O$ (right) together with the assignment of the modes.

Table 3. Variation of the vibrational frequencies in cm^{-1} of silanone for various values of the kinetic energy cutoff E_{cut}.

	E_{cut} (Ha)					
	15	20	25	30	32.5	35
Bending (x–y plane)	638	647	653	651	652	652
Bending (z dir.)	648	655	657	657	657	657
Scissor bending H–Si–H	960	961	962	961	962	962
Stretching Si=O	1150	1183	1195	1196	1196	1196
Stretching sym. H–Si	2109	2107	2110	2110	2111	2111
Stretching asym. H–Si	2137	2137	2140	2140	2140	2141

a_{cell} = 30 a_B for the small clusters to a_{cell} = 40 a_B for the big ones. With this choice, the kinetic energy cutoff of E_{cut} = 17.5 Ha can easily be used for the non-oxidized nanocrystal, whereas E_{cut} = 32.5 Ha for the oxidized one is beyond the computational limits. Thus, we look at the vibrational frequencies for silanone as a function of E_{cut} (see table 3). As noticed from the table, most of the frequencies do not vary significantly with the number of plane waves already from medium values of E_{cut}. The largest variations are found for the stretching Si=O frequency. However, even this frequency is already converged at E_{cut} = 25 Ha. Thus, we could reduce the kinetic energy cutoff for silanone without obtaining significantly different results. In order to see if this conclusion is also true for $Si_{10}H_{14}O$, we have calculated the vibrational spectra at E_{cut} = 15 Ha and at E_{cut} = 25 Ha. For the stretching Si=O we have found a difference of 52 cm^{-1} between these two calculations, which is nearly the same as for silanone, comparing the values at the same kinetic energy cutoffs. Since the other frequencies of $Si_{10}H_{14}O$ did not vary significantly between the calculations using E_{cut} = 15 and 25 Ha, we can assume that convergence has been achieved at 25 Ha. This finding was confirmed, since the vanishing frequencies are lower than 16 cm^{-1}.

4.2. Vibrational density of states

For the big nanocrystals we obtained a large number of frequencies. In the case of $Si_{10}H_{16}$ we have found 78 frequency eigenvalues, where six frequencies vanish. However, most of the modes are twofold or threefold degenerate. For $Si_{10}H_{14}O$ there are 75 frequencies and none of them is degenerate. Thus, we have calculated the vibrational density of states (DOS), where we applied a Gaussian broadening of width 12.8 cm^{-1}. The result is presented in figure 6. To our knowledge, there are no experimental data available for comparison for these two clusters.

Analyzing the DOS for $Si_{10}H_{16}$, we can distinguish four regions: the low-frequency collective Si–Si modes with frequencies up to ≈500 cm^{-1}, from ≈500 cm^{-1} to ≈750 cm^{-1} the Si–H–Si bending and wagging modes, the peak at ≈870 cm^{-1} corresponds to the Si–H–Si scissor-bending modes, and at ≈2100 cm^{-1} we have the Si–H stretching modes. Compared to silane, the Si–H stretching modes have slightly lower frequencies.

In the DOS of $Si_{10}H_{14}O$ we find the same regions for the Si- and Si–H-related vibrations. In addition, we find in the frequency gaps some oxygen-related vibrations: at 234 cm^{-1} a Si=O bending mode and at 1155 cm^{-1} the Si=O stretching mode. These peaks in the DOS are the oxygen signature in the spectra. The Si=O stretching frequency is comparable to that of silanone, which was at 1196 cm^{-1}. For the Si=O bending mode, the displacement of Si and O is similar to the bending x–y mode of silanone; however, it is at a quite different frequency.

We have also compared the DOS of $Si_{10}H_{16}$ with the one of $Si_{10}H_{14}O$. Here we observe that the peak of the Si–H stretching modes and the one of the Si–H–Si scissor-bending modes coincide for both clusters, and thus they are independent of the presence of the oxygen. In contrast, the regions of the Si- and Si–H-related frequencies of $Si_{10}H_{16}$ are slightly different from the ones of $Si_{10}H_{14}O$, since in the latter case there is an overlap with oxygen-related modes. Nevertheless, it would be possible to discriminate experimentally the oxidized nanocrystals from the non-oxidized one due to the characteristic Si=O frequencies.

4.3. Analysis of displacement patterns

After we have identified the characteristic oxygen-related spectral features in the DOS, we also want to analyze the

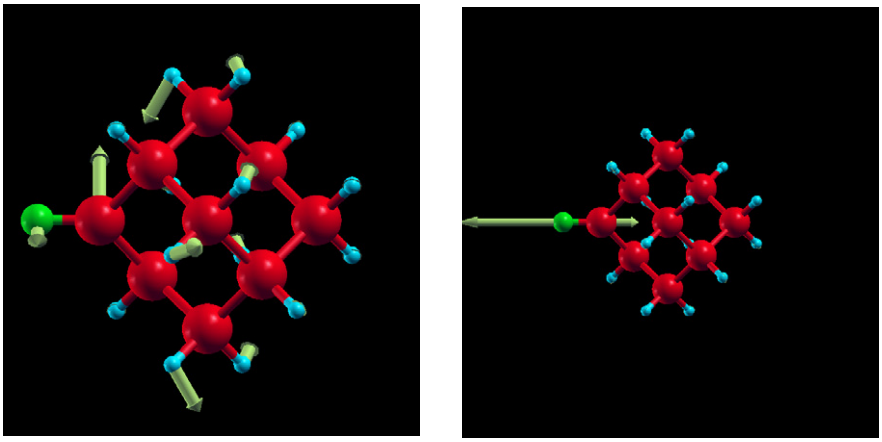

Figure 7. Eigendisplacements of oxygen-related modes, Si=O bending (left) and Si=O stretching (right) modes at frequencies 234 cm^{-1} and 1155 cm^{-1}, respectively.

displacement patterns of the corresponding modes. The eigenvectors of the Si=O bending and the Si=O stretching modes are displayed in figure 7. The Si=O bending mode has a delocalized character, where the Si=O stretching one is completely localized at the oxygen and its neighboring silicon atom. Both modes show no inversion symmetry and are Raman active.

5. Summary and outlook

We have investigated the silicon nanocrystals SiH_4 (silane), H_2SiO (silanone), $Si_{10}H_{16}$, and $Si_{10}H_{14}O$ with respect to their vibrational properties. The vibrational frequencies of silane and silanone are in good agreement with experimental and theoretical reference data. We have computed the vibrational density of states for the non-oxidized $Si_{10}H_{16}$ and the corresponding oxidized one $Si_{10}H_{14}O$ where the oxygen is double bonded to a silicon atom. The frequencies have been analyzed with respect to their vibrational character. For $Si_{10}H_{16}$ we have found four regions related to Si–Si vibrations and various Si–H motions. The same regions are also present in the density of states of the $Si_{10}H_{14}O$ cluster, where we have found additional peaks in the frequency gaps of $Si_{10}H_{16}$. These additional peaks have been identified as a non-localized Si=O bending mode and a localized Si=O stretching mode. Thus, comparing the vibrational density of states of the oxidized and the non-oxidized nanocrystal, we find a clear signature of the oxygen in the spectra.

A further investigation of these nanocrystals will contain an analysis of the vibrational spectra of other $Si_{10}H_{14}O$ isomers, as well as a characterization of localized and non-localized modes and their Raman activity.

Acknowledgments

This work was funded in part by the EU's Sixth Framework Program through the NANOQUANTA Network of Excellence (NMP-4-CT-2004-500198). Computer facilities at CINECA granted by INFM (project no 643/2006) are gratefully acknowledged. We would also like to thank Matteo Gatti, Stefano Ossicini, and Paolo Giannozzi for fruitful discussions.

References

[1] Canham L T 1990 *Appl. Phys. Lett.* **57** 1046
[2] Gatti M and Onida G 2005 *Phys. Rev.* B **72** 045442
[3] Luppi M and Ossicini S 2003 *J. Appl. Phys.* **94** 2130
[4] Luppi M and Ossicini S 2003 *Phys. Status Solidi* a **197** 251
[5] Ossicini S, Iori F, Degoli E, Luppi E, Magri R, Poli R, Cantele G, Trani F and Ninno D 2006 *IEEE J. Sel. Top. Quantum Electron.* **12** 1585
[6] Sychugov I, Juhasz R, Valenta J and Linnros J 2005 *Phys. Rev. Lett.* **94** 087405
[7] http://www.abinit.org
[8] Hohenberg P and Kohn W 1964 *Phys. Rev.* B **136** 864
[9] Kohn W and Sham L J 1965 *Phys. Rev.* A **140** 1133
[10] Troullier N and Martins J L 1991 *Phys. Rev.* B **43** 1993
[11] Perdew J P and Zunger A 1981 *Phys. Rev.* B **23** 5048
[12] Ceperley D M and Alder B J 1980 *Phys. Rev. Lett.* **45** 566
[13] Gonze X and Lee C 1997 *Phys. Rev.* B **55** 10355
[14] Gonze X 1997 *Phys. Rev.* B **55** 10337
[15] Cardona M 1983 *Phys. Status Solidi* b **118** 463
[16] Boyd D C J 1955 *J. Chem. Phys.* **23** 922
[17] Kim E, Lee Y H and Lee J M 1994 *J. Phys.: Condens. Matter* **6** 9561
[18] Min B J, Lee Y H, Wang C Z, Chan C T and Ho K M 1992 *Phys. Rev.* B **45** 6839
[19] Bogey M, Delcroix B, Walters A and Guillemin J C 1996 *J. Mol. Spectrosc.* **175** 421
[20] Withnall R and Andrews L 1985 *J. Phys. Chem.* **89** 3261
[21] Hargittai M and Réffy B 2004 *J. Phys. Chem.* A **108** 10194
[22] Gole J L and Dixon D A 1998 *Phys. Rev.* B **57** 12002
[23] Martin J M L 1998 *J. Phys. Chem.* A **102** 1394
[24] Darling C L and Schlegel H B 1993 *J. Phys. Chem.* **97** 8207
[25] Kudo T and Nagase S 1984 *J. Phys. Chem.* **88** 2833
[26] Ma B and Schaefer H F 1994 *J. Chem. Phys.* **101** 2734
[27] Koput J, Carter S and Handy N C 1999 *Chem. Phys. Lett.* **301** 1
[28] http://www.gaussian.com